CLASSIFICATION OF ACTIVE GALACTIC NUCLEI

Radan, Tamara

Undergraduate thesis / Završni rad

2024

Degree Grantor / Ustanova koja je dodijelila akademski / stručni stupanj: **Josip Juraj Strossmayer University of Osijek, Department of Physics / Sveučilište Josipa Jurja Strossmayera u Osijeku, Odjel za fiziku**

Permanent link / Trajna poveznica: https://urn.nsk.hr/urn:nbn:hr:160:158383

Rights / Prava: In copyright/Zaštićeno autorskim pravom.
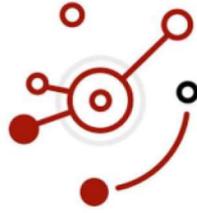
Download date / Datum preuzimanja: **2024-11-27**

Repository / Repozitorij:

Repository of Department of Physics in Osijek

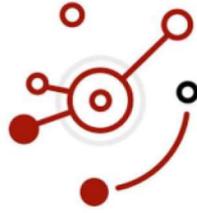**JOSIP JURAJ STROSSMAYER UNIVERSITY OF OSIJEK**
DEPARTMENT OF PHYSICS

TAMARA RADAN

CLASSIFICATION
OF ACTIVE GALACTIC NUCLEI

Bachelor's Thesis

Osijek, 2024.

JOSIP JURAJ STROSSMAYER UNIVERSITY OF OSIJEK
DEPARTMENT OF PHYSICS

TAMARA RADAN

CLASSIFICATION
OF ACTIVE GALACTIC NUCLEI

Bachelor's Thesis

Submitted to the Department of Physics, Josip Juraj Strossmayer University of Osijek, for the academic degree of Bachelor of Physics.

Osijek, 2024.

"This thesis was made under the supervision of Assistant Professor Dario Hrupec and Jelena Strišković, mag. educ. phys. et inf., at the Department of Physics of University of Josip Juraj Strossmayer in Osijek, as a part of the undergraduate program in physics."

KLASIFIKACIJA AKTIVNIH GALAKTIČKIH JEZGRI

TAMARA RADAN

Sažetak

U ovom završnom radu predstavljene su aktivne galaktičke jezgre, njihova svojstva, kao i različitite klasifikacijske sheme. Prvi dio, objašnjava što su aktivne galaktičke jezgre. Drugi dio objašnjava njihova svojstva i fizikalne mehanizme potrebne za njihovo razumijevanje na preddiplomskoj razini. U radu je dan i povijesni pregled klasifikacije aktivnih galaktičkih jezgara kao i dva najpoznatija pokušaja klasifikacije: Fanaroff-Riley klasifikacija i unificirane sheme temeljene na orijentaciji. Na kraju su prikazani viševalne svjetlosne krivulje kao i spektralna raspodjela energije jedne aktivne galaktičke jezgre, blazara S4 0954+65.

CLASSIFICATION OF ACTIVE GALACTIC NUCLEI

TAMARA RADAN

Abstract

In this Bachelor's Thesis, active galactic nuclei (AGN), their properties, as well as different classification schemes are presented. The first part explains what active galactic nuclei are. The second part explains their properties and the physical mechanisms necessary for their understanding at the undergraduate level. The thesis also provides a historical overview of the classification of active galactic nuclei as well as the two most famous classification attempts: Fanaroff-Riley classification and Unified schemes based on orientation. Finally, multiwavelength light curves are shown as well as the spectral energy distribution of a spesific active galactic nucleus, the blazar S4 0954+65.

Contents

1 Introduction

Active Galactic Nucleus (AGN) is an active black hole located in the center of some galaxies. Main characteristic of such objects is that, unlike galaxies that have non-active nuclei, which only have an absorption spectrum that is given by the light from the stars within these galaxies, AGNs also, at the same time, show broad-band emission lines in multiple frequencies. Because of the high polarisation of the waves, and the characteristic power-law of AGN radio spectrum, scientists realised the reason behind these emissions was synchrotron radiation from charged particles traveling at relativistic speeds. Given particles were accelerated by the magnetic field of the source, and followed a spiral path around the field's direction. It was also discovered that majority of radio waves in these sources are coming from 2 symmetrical lobes around the galactic center, each on the opposite side and pointing along the axis perpendicular to the galactic disk, which gave us a hint about the physical structure of AGN objects. Despite differences in the spectra, many different objects like Seyfert galaxies, quasars, blazars, etc. are all classified as AGNs. The questions we ask here is: why do all AGNs in general look so similar, especially in comparison to the normal, non active, galactic nuclei, but are still showing some major differences within the class. Here we will discuss different classification schemes that will help us answer these questions.
[7, chapter 8.1] [6, page 550]

2 Theoretical Part

2.1 Physics of AGNs

2.1.1 Spectroscopy, Emission and Absorption of Light

To understand the physics of AGNs we need to take a closer look at certain properties of light. Visible light is just one small window of the electromagnetic spectrum, covering wavelengths from $400\,\mathrm{nm}$, that is, the equivalent of violet light, all the way up to around $700\,\mathrm{nm}$, the equivalent of red light. The light can be described as waves and as particles. Single light particle is called a photon. And photons are massless particles that carry certain amount of energy. Maxwell's equations very neatly describe light in the context of propagation of electromagnetic (EM) radiation. Equations say that a changing electric field causes a magnetic field, and that a changing magnetic field causes an electric field. Whichever one happens first, causes the other, and the process repeats itself, creating waves consisting of oscillating electric and magnetic fields, called EM waves. All waves in general are described by three independent quantities: amplitude, speed, and frequency. Amplitude is height above undisturbed position, speed here refers to the speed of propagation of the wave denoted by c in case of the speed of light, and v in case of the mechanical waves. Frequency, denoted by f, is the number of wave peaks crossing a point in space each second. Frequency and speed of the wave are connected through relation $f = v/\lambda$. Wavelength, denoted by λ, is the distance from one peak to the next. In special case of the EM waves moving through vacuum, the equation becomes: $f = c/\lambda$, and that same EM wave carries an energy $E = hf = hv/\lambda$, where h denotes Planck's constant $h = 6.6260715 \times 10^{-34}\mathrm{JHz}^{-1}$. Colours of the visible light are actually just different frequencies of the given light. We already mentioned that visible frequencies don't represent the full range of possible frequencies of EM radiation. Maxwell's equations actually place no restrictions on the wavelengths of the waves. Equations also predict the speed of EM wave propagation, and this prediction agrees with the modern measurement of the speed of light that gives a value of $c = 299\,792\,458\,\mathrm{m\,s}^{-1} \approx 3 \times 10^5\,\mathrm{km\,s}^{-1}$ in a vacuum. [6, page 113]
Spectral analysis was first done by strong magnification and analysis of the solar spectrum. The
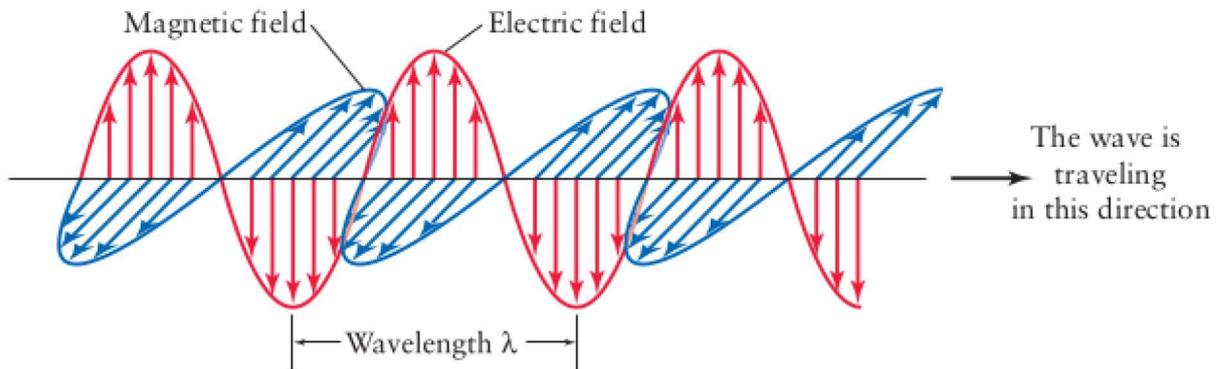
Figure 1: Electromagnetic wave
[13, page 103]

lines shown were an absorption lines of a different elements that light has passed through. Before this discovery, everything we knew from observing the incoming light was about the light itself and its properties, but this was the first time that the light has revealed the information about the objects interacting with it. Kirchhoff and Bunsen later found that each chemical element shows its own unique pattern, of spectral lines, by which it can be identified, just like fingerprints that uniquely identify individual persons.

Kirchhoff specifically described his findings in 3 laws:

- The 1st law states that an opaque and at the same time dense gas produces a continuous spectrum without spectral lines, and the ideal case of such a body is called a black-body.

- The 2nd law states that a gas that is transparent and hot at the same time, produces bright emission lines of a given element that the gas is made of.

- The 3rd law states that a gas that is transparent and cool at the same time, produces dark absorption lines of a given element that gas is made of. The absorption and emission lines of a given element are of the same frequencies.

A graphical representation of the laws is shown in Figure 2. These laws are important for discussing properties of AGNs. [6, page 111]

We still didn't explicitly say what emission or absorption lines of different atoms and molecules represent. Electrons in an atom have different discrete energy states. The lowest possible one is called ground state, denoted by E_0, any higher or excited energy state is a multiple of the ground state.

When the energy state changes, the atom absorbs or emits a photon that has the same energy as one of the multiples of the ground state. For example: $E_{photon} = E_3 - E_2$ is a transition from third excited state to the second. In this transition, a photon that is giving the energy to the atom is exactly E_0. Absorption lines are visible holes in the continuous spectrum left by the absorption of photons of specific frequency by the atom. Emission lines are lines of the same frequency as would be the absorption lines of the same element, but they appear as coloured lines emitting those specific frequencies of light on a black background.

Figure 2: Kirchoff's laws
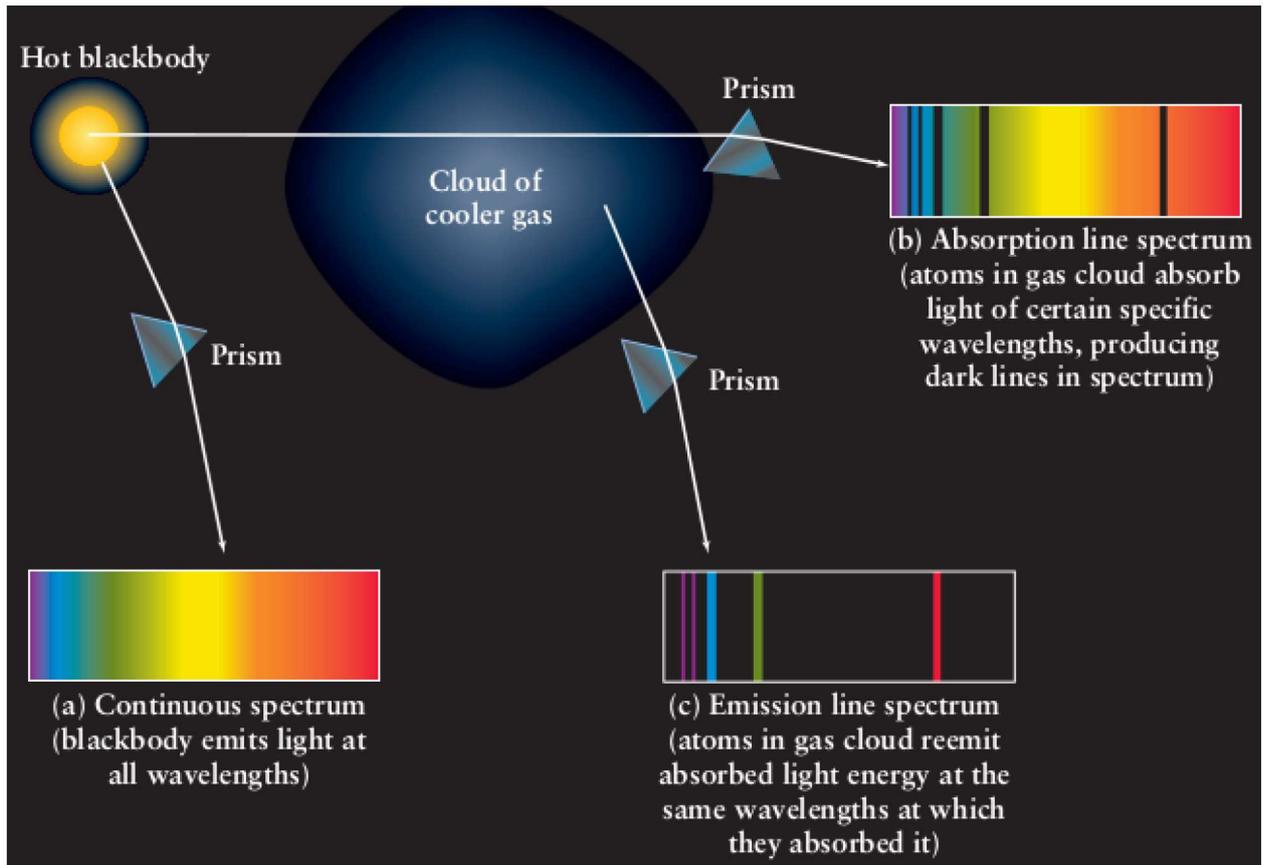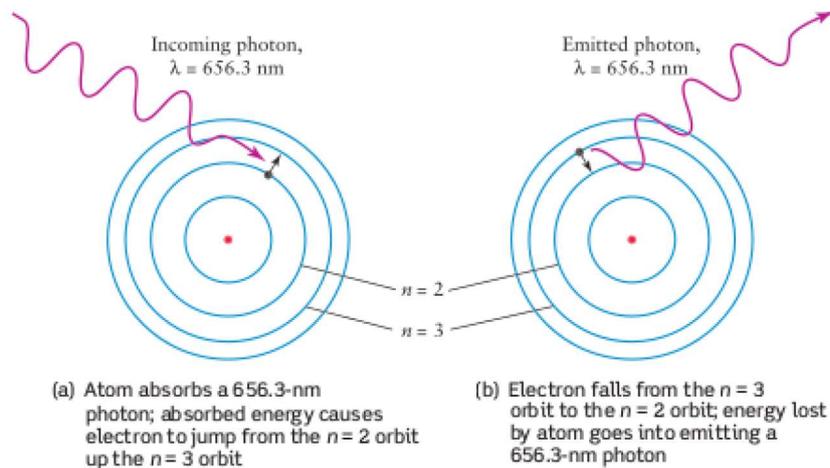[13, page 113]

Figure 3: absorption and emission of photon
[13, page 118]

2.1.2 Doppler Effect

Our perception of frequency of the traveling incoming wave changes depending of how the source is moving relative to us. This happens because in the case of moving towards/away from the observer, each next wave peak is emitted from a position a little bit closer to/further away from the

3

person, so observer detects a shorter/longer wavelength, than he would if the source were stationary. The wavelength shift also means shift in the colour of the light, and because of that shortening of the wavelength is called the blueshift, while move towards longer wavelengths is called the redshift. This phenomena is called the Doppler effect, after the scientist who first described it. Equation for linear movement is: $\delta\lambda/\lambda_0 = v/c$, where $\delta\lambda$ is wavelength shift, λ_0 is wavelength if source is not moving, v is velocity of the source measured along the line of sight, and c is speed of light. But what happens if the wave source is rotating instead of moving in line? One side is from our perspective moving towards us, and the other one away. This type of Doppler shift caused by the rotation of an object will help us detect and describe certain parts of AGNs, and here is the figure to better understand the problem.
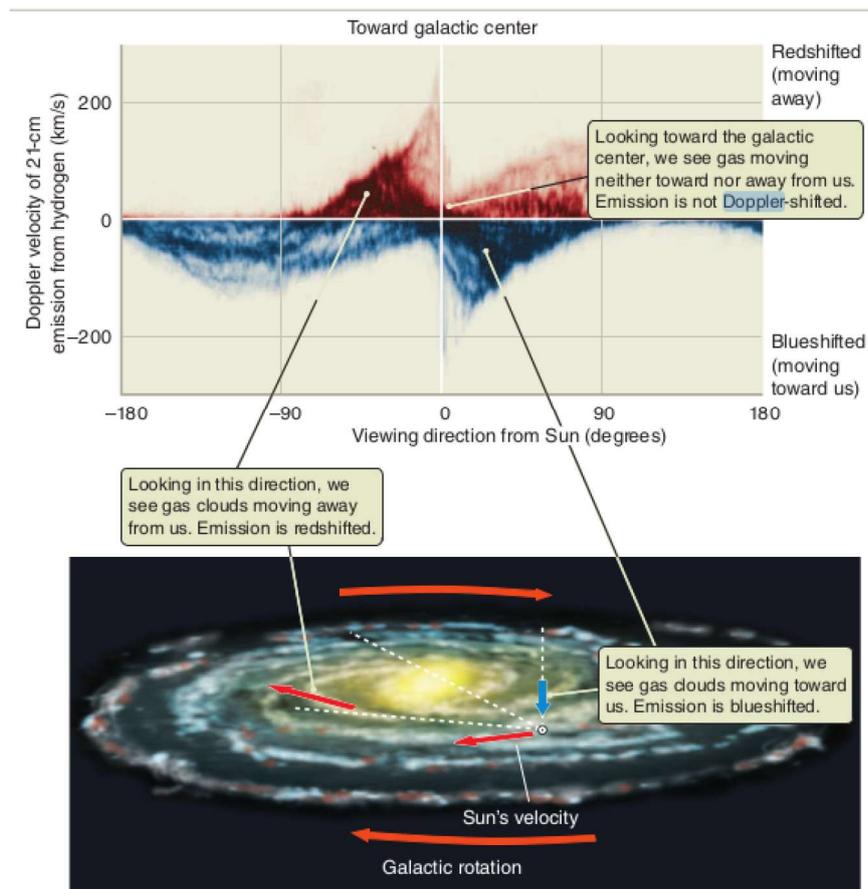
Figure 4: Doppler shift of the rotating galaxy
[6, page 577]

The Doppler shift provides information only about the radial velocity (v_r) of the object, which is the part of the motion that is toward you or away from us. If we are the far away observer on the left center of this figure, from our perspective rotating gas has a different Doppler shift on the opposite sides. That is because while rotating, gas on one side moves away from us, and on the opposite side towards us.
[6, page 126] [13, page 123]

2.1.3 Compton Scattering

Compton scattering is a process in which a high energy photon, during its journey, encounters a static electron, and by colliding with it, partially transfers its energy and momentum onto the given

electron. The scattered electron has a lower energy and momentum than before the event took place. From the Planck-Einstein relation $E = \hbar\omega$ we know that the energy of a photon depends on its frequency ω and so if we take into account that momentum is directly proportional to the energy $p = E/c$,we see that momentum is also directly proportional to the frequency through the same relation. [7, page 232]
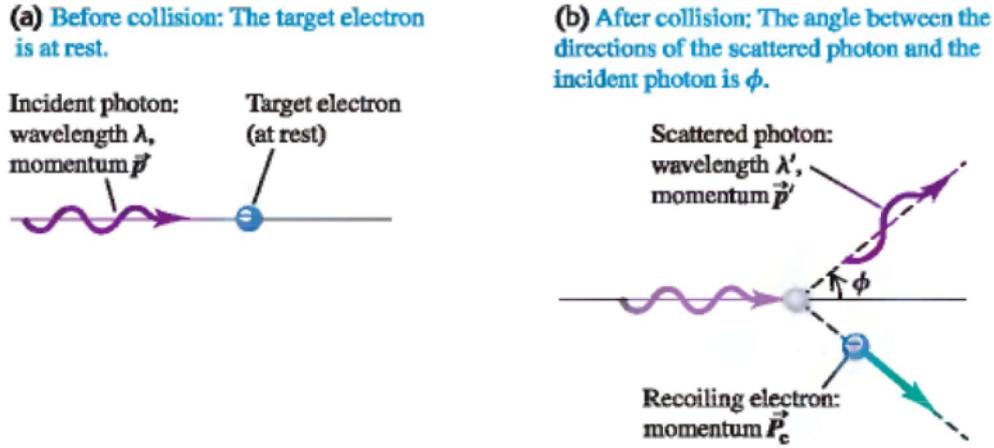
Figure 5: Compton scattering
[20, page 1333]

We shall mark the momentum and the energy of the photon before the scattering with **p** and pc respectively, while the moment and the energy after are marked **p'** and $p'c$ respectively. Initially, the electron is at rest, and because of that, its initial momentum was zero, and at the same time its energy consisted only of its rest mass, mc^2. The final momentum of the electron is $\mathbf{P}_e$, and at the same time, its energy is $E_e = (mc^2)^2 + (P_e c)^2$. From energy conservation we obtain:

$$pc + mc^2 = p'c + E_e$$

and therefore:

$$(pc - p'c + mc^2)^2 = Ec^2 = (mc^2)^2 + (P_e c)^2$$

If we eliminate $\mathbf{P}_e$ with the use of conservation of momentum:

$$\mathbf{p} = \mathbf{p'} + \mathbf{P}_e$$
$$\mathbf{P}_e = \mathbf{p} - \mathbf{p'}$$

and than we shuffle the terms in the equation:

$$p^2 c^2 + p'^2 c^2 + m^2 c^2 + 2pmc^3 - 2pp'c^2 - 2p'mc^3 = m^2 c^2 + p^2 + p'^2 + p'^2 - 2pp' \cos\theta$$

Some terms cancel out and we get:

$$pmc - pp' - p'mc = -2pp' \cos\theta \tag{1}$$

$$\frac{mc}{p'} - \frac{mc}{p} = 1 - \cos\theta \tag{2}$$

Since $p = \frac{h}{\lambda}$ and $p' = \frac{h}{\lambda'}$,with substitution we get the final expression for the difference in wavelength between the photon before and after the collision:

5

$$\boxed{\lambda' - \lambda = \frac{h}{mc}(1 - \cos\theta)} \tag{3}$$

[20, page 1333]

The described process can also go the other way around, where instead static electrons, we have ultra-relativistic electrons that scatter low energy photons to high energies. Here the photons gain energy while decreasing the kinetic energy of the electrons.

2.1.4 Syncrothron Radiation
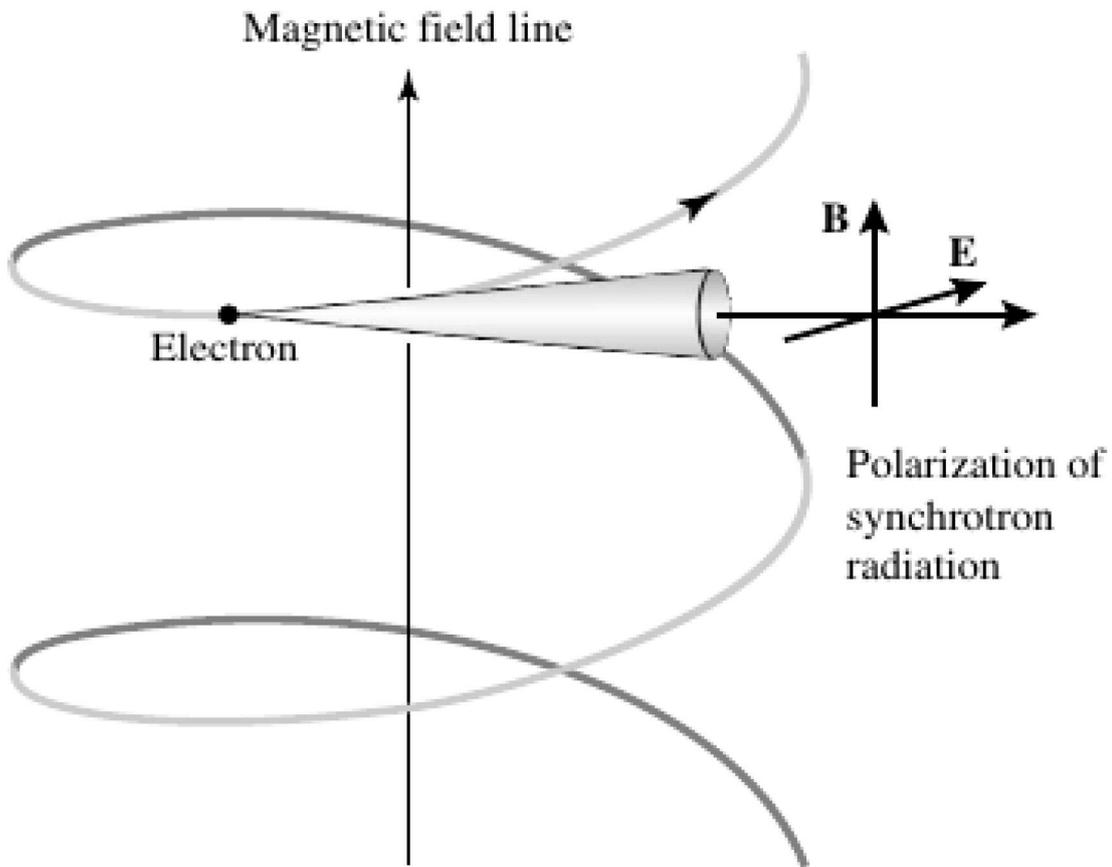
Figure 6: Electron spirals as it gets accelerated by the magnetic field and emits synchrotron radiation

[4, page 653]

Synchrotron radiation is a product of relativistic electrons spiraling along magnetic field lines. While spiraling they accelerate and emit EM waves that we can later detect and analyse the spectrum. Magnetic force on a moving charge q is: $\vec{F_m} = q(\vec{v} \times \vec{B})$

The component of an electron's velocity that is perpendicular to the lines of the magnetic field is responsible for the circular motion around the field lines. If this component dominates, the radiation is called synchrotron radiation. Meanwhile, if the parallel component is the dominant one, the radiation is called curvature radiation. The shape of the continuous spectrum that is produced, will depend on the energy distribution of the emitting electrons. The two types of

radiation are both linearly polarised, but in different planes. Synchrotron radiation is polarised in the plane of the circular motion, and curvature radiation in the plane of the magnetic field. [4, page 625]

2.1.5 Spectral Energy distribution of AGNs

Figure 7: On the left side is the spectrum of the Sun taken through the window, and the right side is SED of AGN

[4, page 1190]

Right side of the figure shows an approximation of schematic of the continuum observed for lots of types of AGNs and it's full name is Spectral Energy Distribution (SED) of AGN. Vertical axis on thi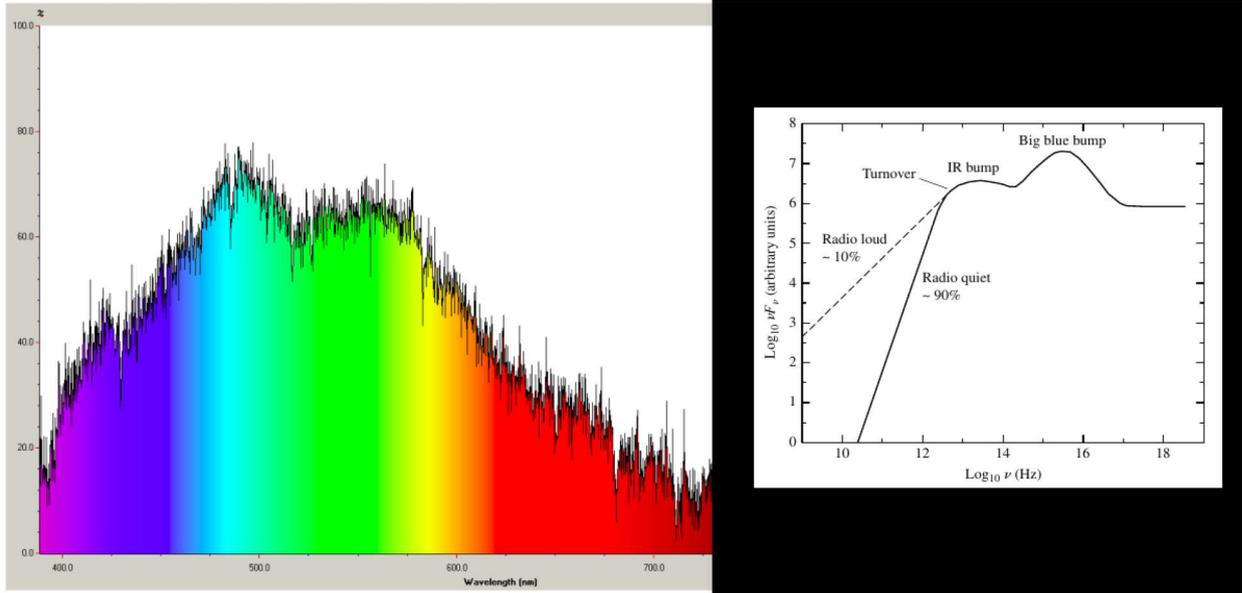s plot is logarithm of the product fF_f which we will explain in awhile. The SED covers huge range of frequencies which makes it different from the blackbody radiation, or some other, spectrum. On the left side is the spectrum of the Sun taken through the window of a classroom. This slightly changes peak frequency from green to light blue part of the spectra, but even with this slight change, spectrum is obviously more limited in scale of frequencies in which it's strong. Vertical axis shows how strong each of the frequencies is. We can see, on the Sun's spectrum, huge drop in power where visible frequencies begin and end. On the other hand, SED covers huge part of the EM spectrum. In the early days of AGN research, it was thought that their spectra were pretty flat. Because of that, a power law of the form $F_f \propto f^{-\alpha}$, at the time, was used to show the energy flux - the amount of energy in frequency interval $f + \Delta f$ that passes through the cross section in 1 sec. time interval. The spectral index denoted by α, at the time was thought to have the value $alpha \simeq 1$ The power within any frequency interval from f_1 to f_2 is:

$$L_{interval} \approx \int_{f_1}^{f_2} F_f \, df = \int_{f_1}^{f_2} f F_f \, (df/f) = \ln 10 \int_{f_1}^{f_2} f F_f \, d\log_{10} f \qquad (4)$$

Equal areas under a graph of fF_f vs. $\log_{10} f$ correspond to equal amounts of energy, and that gives us a reason for plotting the ordinate in a form that is shown. Dotted line shows steepness of radio spectrum of radio loud AGNs, while non dotted line on the left of the IR bump shows steepness and the beginning of detectable frequencies of the radio quiet AGNs. A value of $\alpha \simeq 1$
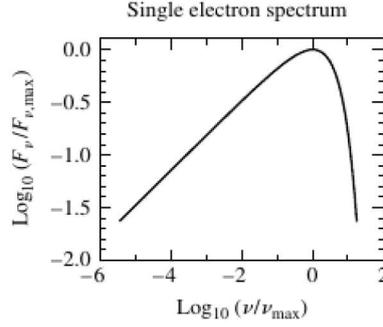
7

Figure 8: Spectrum of a single electron that obeys power law $F_f \propto f^{-\alpha}$
[4, page 1191]

reflects the horizontal trend seen to the right of the turnover in the plot for SED. The spectral index usually has a value between 0.5 and 2 that mostly increases with increasing frequency, so shown plot has a concave shape. That makes it frequency variable that is constant over smaller intervals of frequecies. This plot can occasionally be decomposed into two separate contributions: first one from thermal sources, such as black body spectrum with low polarization, and second one from the non-thermal sources, such as power-law spectrum with significant polarization. The thermal component appears as the big blue bump which is here probably due to an optically thick accretion disk around nuclei. We can also see the thermal infrared bump to the left of the big blue bump which it is probably due to emission from warm dust grains. All of these pieces give us a better understanding of the structure of AGNs. Power-law spectrum that has constant α is the signature feature of synchrotron radiation. The distribution of the individual electron energies is described by already given power law: $F_f \propto f^{-\alpha}$ We can see that in reality, the synchrotron spectrum does not continue to rise limitlessly as the frequency decreases. At some transition frequency, the spectrum turns over and varies as $f^{5/2}$. The reason is because the plasma of the spiraling electrons becomes opaque to its own synchrotron radiation, which dampens the signal. This effect is called synchrotron self-absorption. [4, page 1189]

2.1.6   Syncrothron Self-absorption

Lets take a closer look at the effect we just mentioned, and understand the reasons for turn over from $f^{-\alpha}$ to $f^{5/2}$. Let's assume we again have power law in the same form as before: $F_f \propto f^{-\alpha}$, and take spectral index of this source to be $\alpha = (p-1)/2$. Let's also assume that this source has the same size at all frequencies. That means so that it's brightness temperature: $T_b = (\lambda^2/2k)(F_f/\Omega)$ is proportional to $f^{-(2+\alpha)}$ where F_f is it's flux density and Ω is the solid angle between the observer and the source. T_b is fined using the expression for the intensity I_f of black body radiation: $I_f = F_f/\Omega = (2hf^3/c^2)(exp^{1-(hf/kT_b)})$ which is approximately $(2kT_B)/\lambda^2$ in Rayleigh-Jeans limit. T_b is a lower limit to the regional temperature, because no region can emit continuum of higher intensity than the one of a blackbody. Most often for the radio sources we have $\alpha \approx 1$. At longer wavelengths, T_b of the radiation may approach the temperature of the radiating electrons. And here, self-absorption effects become important. Synchrotron radiation spectrum of F_f for relativistic electrons is $N(E)dE = \kappa E^{-p}dE$ This energy spectrum doesn't represent thermal equilibrium but we can still use the term temperature because the emission spectrum of electrons of energy E has a peak around the critical frequency $f \approx f_c$, so the opposite processes of emission and absorption of a photon at some f, have electrons of almost the same energy. And also, since the electron number densities are very low, and time scale for matter interactions is very
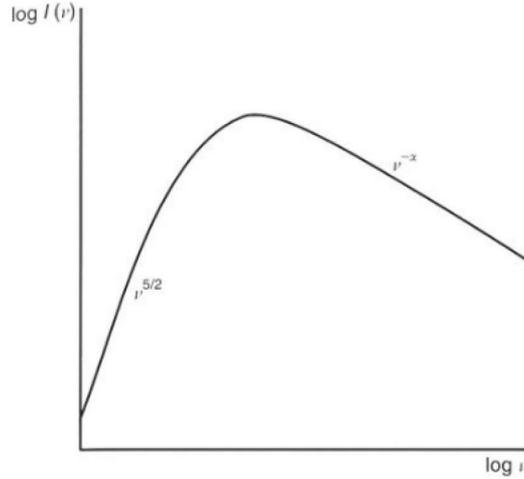
The spectrum of a source of synchrotron radiation which exhibits the phenomenon of synchrotron self-absorption.

Figure 9: $\nu^{-\alpha}$ on this graph is the power law that we denoted by $f^{-\alpha}$
[7, page 219]

big, T_e, the energy of electrons is gained from relativistic form of formula: $\gamma m_e c^2 = 3kT_e$
The ratio of specific heat capacities γ_{SH} is $4/3$ for a relativistic gas. The internal thermal energy density of a gas is $u = NkT/(\gamma_{SH} - 1)$, and here, N is the number density of electrons. By tweaking γ_{SH} we get different results. For $\gamma_{SH} = 5/3$ we get the classical one $E = (3/2)kT_e$ and by setting $\gamma_{SH} = 4/3$, we get the expression $\gamma m_e c^2 = 3kT_e$. Because of this, T_e of the electrons becomes a function of their energy. Since $\gamma \approx (f/f_g)^{1/2}$, where f_g is a non-relativistic gyrofrequency, frequency at which most of the radiation is emitted, we get: $T_e \approx (m_e c^2/3k)(f/f_g)^{1/2}$. For a self-absorbed source $T_b = T_e$ so, in the Rayleigh–Jeans limit:
$F_f = (2kT_e/\lambda^2)\Omega = (2m_e/3f_g^{1/2})\Omega f^{5/2} \propto (\theta^2 f^{5/2})/B^{1/2}$. Here, Ω is the solid angle taken by the source $\Omega \approx \theta^2$ and θ is the angular size of the source. This shows us the physical reason for the steep spectrum at bigger wavelengths found in objects with synchrotron self-absorption, that have $F_f \propto f^{5/2}$. This does not follow the Rayleigh–Jeans law because T_e of the electrons shows great variability depending on wavelength. Spectra similar to this form is found for most AGNs. This provides strong evidence for the presence of relativistic electrons coming from the nucleus. Important fact is also that radiation going through the process of self-absorption shows lower levels of linear polarisation in comparison to regular synchrotron radiation from the nucleus. This helps explain low polarisation of radiation coming from core dominant AGNs. [7, chapter 8.7]

2.2 Historical AGN Types

2.2.1 Seyfert Galaxies

The optical range was the first one to be observed, so first AGNs detected were observed in it and looked similar to nebulas, and were wrongly classified as Spiral Nebulas. Today, the percentage of AGNs classified as Seyfert galaxies can vary depending on the sample and the criteria used for classification, but Seyferts are actually not that common, and percentage wise, most likely around $10\% - 20\%$ of AGNs are Seyferts. Equally interesting is that around 90% of the close to us Seyferts are spiral galaxies. Carl Seyfert divided the objects into two classes that today are called Seyfert I, and Seyfert II galaxies. The main difference between the two types is the width of their permitted

9

emission lines. Forbidden lines in reality are just low-probability transitions in atoms that also tell us about low gas densities in the regions emitting such lines.

Seyfert 1 galaxies

- Show very broad emission lines, with allowed or permitted lines (HI, HeI, HeII) being even more extremely broadened than the ones from the forbidden transitions, like (OIII)

- Permitted line velocities usually go from 1000 to 5000 $\mathrm{km\,s^{-1}}$ in some extremes can go up to 10 000 $\mathrm{km\,s^{-1}}$

- Higher rotational speed means that the gas is closer to the center of rotation

- Contains non thermal continuum without lines, here more luminous than in 2nd type of Seyferts

Seyfert II

- Only narrow, permitted and forbidden, lines

- Lines of lower velocities, around 500 $\mathrm{km\,s^{-1}}$

- Lower velocities structurally mean that the gas in these objects is in the outer perimeter of the object, meaning further away from the rotational center

- Continuum of lower intensity present, explains lower luminosity in this type

Khachikian and Weedman in the 1970s showed these significant differences in the widths of the emission lines among the Seyferts.

Besides Seyfert I and Seyfert II types, there is a certain number of galaxies that would best be described as Seyfert type 1.5, because of the presence of both broad and narrow permitted lines. They make up minority of Seyferts and were discovered later than both traditional types. The permitted lines can sometimes consist of two components, the standard broad permitted lines of the Seyfert I spectrum, and on top of it a narrow line, typical for Seyfert II spectrum. The spectra of some Seyfert galaxies also shows great time variability of the type, which changes from type 1.5 to type 2 in a matter of years. These galaxies have broader classification, and now we have the full spectrum of Seyfert types (for example we also have Seyfert 1.8 type). At the same time scale, broad H_α emission line has rarely completely disappeared from these variable spectra. This already shows how classification of AGNs is not as easy and straightforward as it seems at first. [7, page 595] [4, page 1187]

2.2.2 Quasars

Some of the first radio objects found were very much star-like, but at the same time were showing strangely broad emissions. Because of this star-like appearance and unusual broad emissions, these objects became known as quasi-stellar radio sources or short quasars. In 1963, Maarten Schmidt noticed a pattern in unusual broad spectrum lines of the object 3C 273 (see Figure 11), and realised these lines actually looked exactly like hydrogen Balmer emission lines, but in the 'wrong' part of the spectrum. They were redshifted ($z = 0.158$) to unfamiliar frequencies.

Gigantic cosmological redshift of quasars speak of the enormous distance between us and these types of sources. In order for these distant types of AGNs to be detectable from the huge distances,
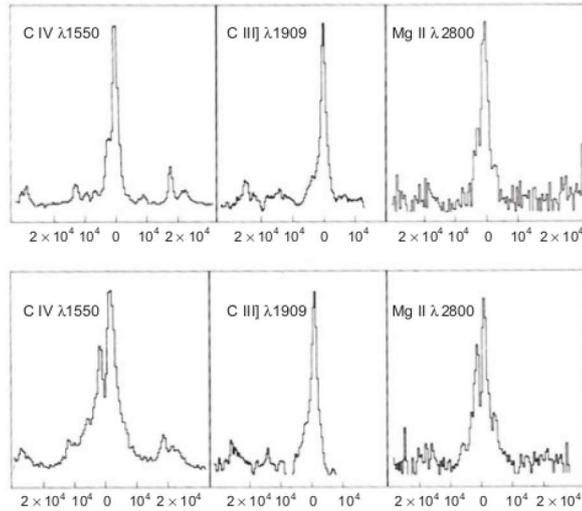
Figure 10: Time variability of Seyfert 1 galaxy lines: Top row was taken in February 1978 and the lower one in June 1980. The UV continuum intensity relatively increased over given period. The C IV and Mg II permitted lines changed a lot over given time period, while the forbidden line [C III] is almost unchanged.

[7, page 595]
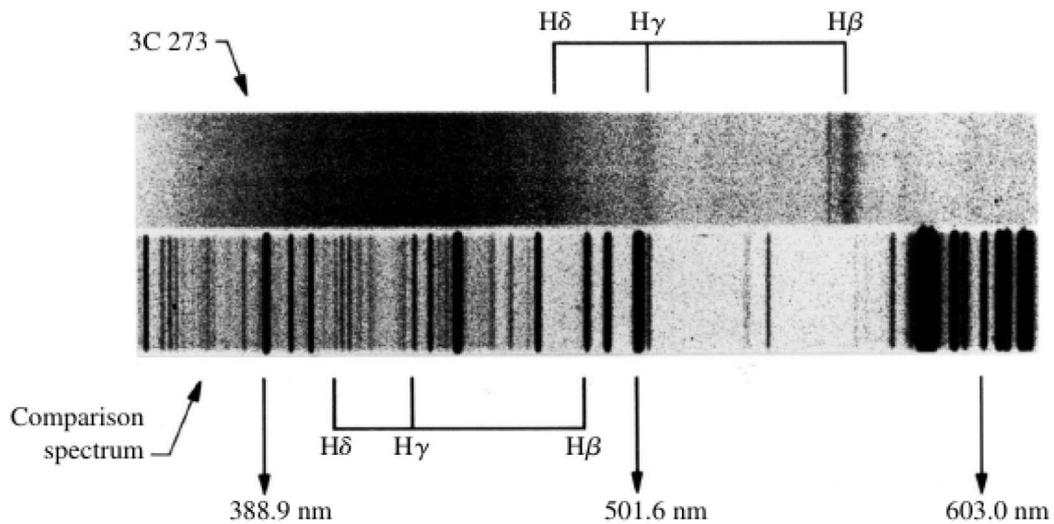
Figure 11: Redshifted spectral lines of Quasar 3C 273, redshift $z = 0.158$
[4, page 1198]

they must be strikingly strong sources. We can divide quasars into two types based on the loudness of their radio emissions.

Radio Loud Quasars

- They have highly strong emissions in the radio part of the spectrum

- Because of the radio loudness were first detected among the quasars

- In reality not a lot of quasars are radio loud, around 10%. The reason is the need for extremely supermassive black hole for this kind of radio loudness, which is also rarity in itself.

- Easier to differentiate from the stars because of the radio loudness

Radio Quiet Quasars

- Lower intensity of radio emissions

- Higher count of this type, because it requires smaller black hole

- Look very similar to stars, except for the higher intensity of UV radiation, which can be used as useful information in finding these quasars

- Big blue bump (BBB) in the SED of quasar visualises this UV loudness

(see Figure 12)

That last couple of facts mean that finding this BBB is a neat technique for finding radio quite quasars and differentiating them from the stars. One of the surveys used scans of plates, previously taken by the telescope, to find this peak in UV radiation of 25 000 quasars by this technique. In the figure we can see the stacked spectra. see Figure 13. The wavelength is plotted on the horizontal axis, and the redshift on the ordinate. Here, we can see the dominant emission lines of [Mg II, C III], [C IV] and Ly_α in quasar spectra. The lines are very redshifted though the optical part of the spectrum. For the reference, Ly_α is normally of frequency 121.567 nm , and belongs to the UV part of the spectrum. Many, even more refined, improved versions of this technique were later developed for the more precise surveys that give better results, but this basic one was explained here to give us a glimpse of how these radio quite quasars are found. [4] (Carroll, 1197)

Not to forget, another greatly important trait of the quasars is their strong variability over smaller and larger time scales, all the way from a day or two, up to a few dozens of years. On this larger time scale, all the quasars that were found up until today, are variable. This is also very helpful in surveys that aim at long term search and cataloging of this type of AGNs. What is also interesting finding is that the amplitude of variability of the quasi stellar AGNs inversely correlates with its luminosity, but does not at all with its redshift. [7, chapter 18.3] [5, chapter 4, Discussion]

2.2.3 Radio Galaxies

Radio galaxies (RGs) are the strongest radio sources outside of the Milky Way. Similar to Seyfert galaxies, we can divide these objects into two classes by the width of their emission lines. Again, the first one being broad-line radio galaxies (BLRGs), which correspond to Seyfert I galaxies, and narrow-line radio galaxies (NLRGs), that correspond to Seyfert II type galaxies. We have some obvious differences between Seyferts and RGs, so what are they?

- Seyfert galaxies nuclei are a lot more quiet within the radio part of the spectrum in comparison to the radio galaxies.

- The second big difference is that nearly all of the Seyfert galaxies fall into the category of spiral galaxies, while stronger RGs are giant or supergiant elliptical galaxies by type.

- Most radio galaxies show low levels of optical non-thermal radiation coming from the nuclei, while Seyferts are known by the strong H_α and other lines in the optical range. [4, page 1194]

- For RGs, the broad lines are usually broader than those found in the spectra of Seyfert I type
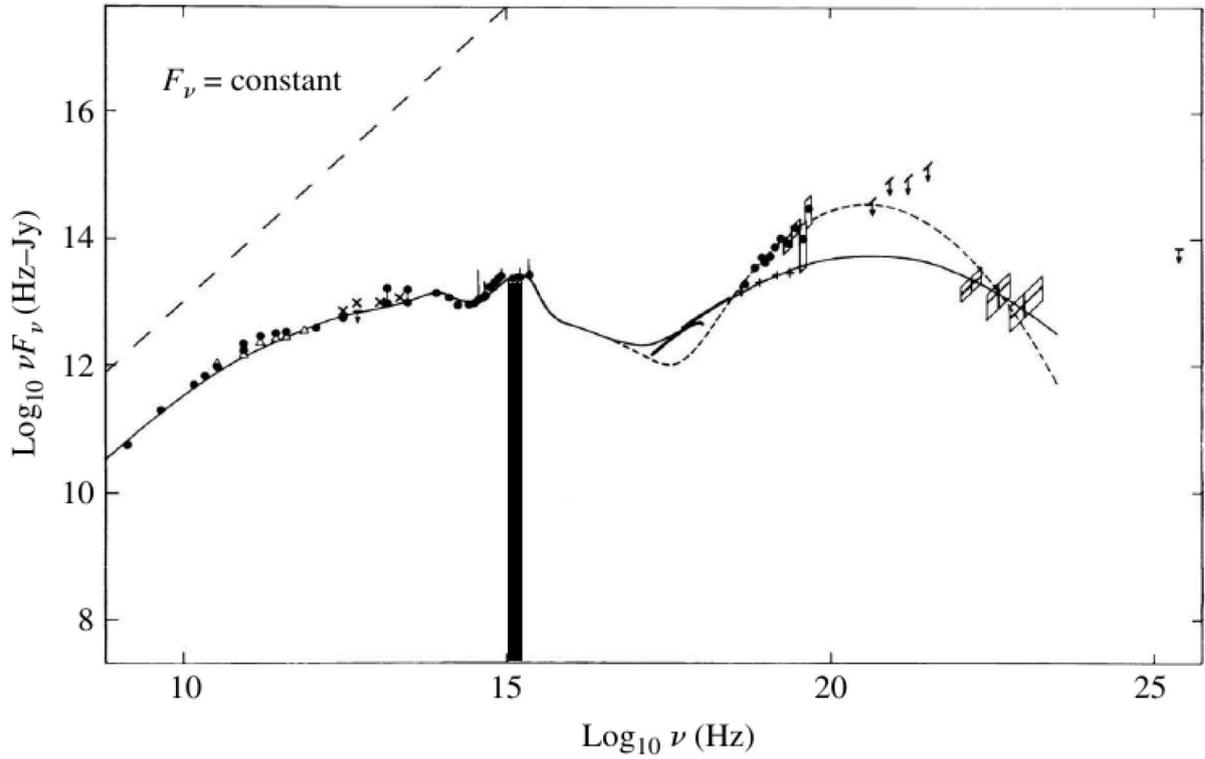
Figure 12: Big blue bump of quasar 3C 273, frequencies of the bump are indicated by thick black vertical line

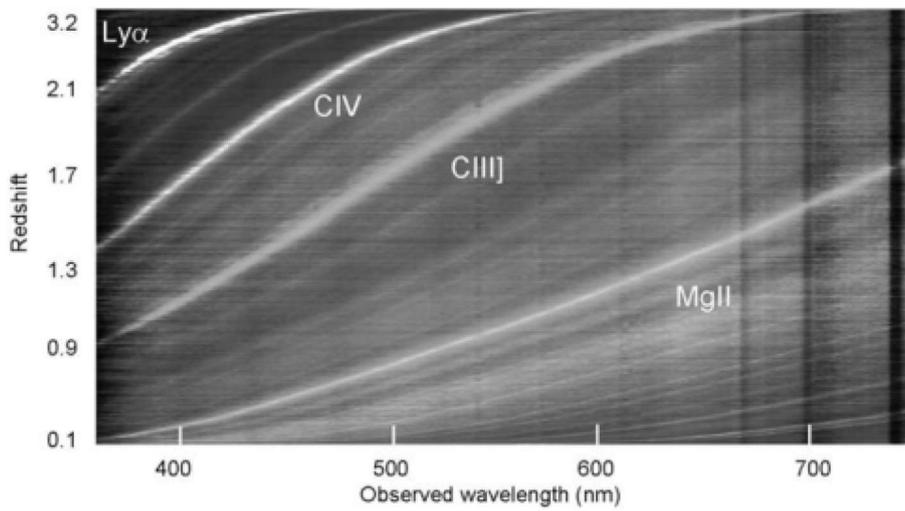[4, page 1200]

Figure 13: Stacked spectra from the 2dF Quasar Survey. It got stacked in order of redshift from z = 0.1 to z = 3.2.

[7, page 590]

- [Fe II] emissions are much stronger in the Seyferts than BLRGs

[7, chapter 18.4, page 595]

13

Lobes and Jets

A lot of RGs show extended features that are not part of their nucleus. These features are also present in some quasars. In fact, quasar's radio emission is either from radio lobes or from a central source in its core. And first of these features we will talk about are lobes. They are single or double sided symmetrical ellipsoidal radio features that extend away from the nuclei of some RGs. Lobes are connected to the galaxy by the collimated jet of particles coming from the nucleus. The jest are a second extended feature we need to discuss, and we have a lot of reasons for that.

Figure 14: RG Centaurus A in optical spectrum with contours of lobes and the jet.

More than $\frac{1}{2}$ of the strong radio galaxies are showing, in these cases mostly one-sided, feature. At the same time, over $\frac{3}{4}$ of the quieter ones, are also showing jets, but this time mostly double-sided ones. [4, page] Because of the high blueshift, the jet pointed towards the observer is very likely to be detected. The stronger galaxies can be detected from enormous distances, and so, on various occasions, the seemingly weaker jet goes undetected, or very weakly detected. Good example of one such galaxy is M87 that has one stronger jet which extends from the center of the galaxy up until the radio lobe. And also has a second dimmer one, which extends away from the galaxy in the opposite direction, but on the same axis as the stronger one. The radiation from the jets is linearly polarised. Jet emissions are caused by synchrotron emission from the central region of AGN. Important to mention is also that the radio jets are not always straight in line and are sometimes showing slightly twisted or disturbed appearance. Mostly this happens because of the galaxy's gravitational interaction with the interstellar gas in the close by area. (Dodat dio koji detaljnije kaze zasto imamo jet i lobes iz izmjenjenog dila iz Caroll 1227 str. Accelerating the

Charged Particles in the Jets, jako lipo je tamo objasnjeno) [4, pages 1194, 1195]
(bez dodanog dila koji bi dodala sa strana 1224-1227) [4, Radio lobes and Jets, from page 1224]

2.2.4 Blasars and Other Strong γ Sources

Some AGNs detected at lower radio frequencies have very flat spectra in that area, $F_f \propto f^0$. As the surveys got better and expand in range, frequencies of the observed flat spectra were higher and higher. These objects all have tiny angular size and show variability on different time scales, from months until years. The size of these sources was measured by very long baseline interferometry (VLBI), a technique that uses multiple smaller radio telescopes that do survey at the same time. The telescopes make an array that acts as one giant telescope whose size is equal to the biggest separation of the individual telescopes in a given array, giving better resolution. Using this technique meant that the measurements of the brightness temperatures for the smallest sources in a bunch, that measured $T_b = (\lambda^2/2k)(S_\nu/\theta^2) \geq 10^{10}$ K, was pretty accurate. And that high temperature implied that the emitting electrons had to be relativistic. The final flat spectrum is the superposition of the spectra of the synchrotron self-absorption at high radio frequencies, gathered from multiple monitored sources. [7, chapter 18.5]

BL Lac

Lots of these objects, smaller in angular size, were found to be quasars, and a smaller group was first thought to be variable stars, but turned out to be AGN, BL Lacertae, or BL Lac. The optical spectrum of BL Lac is very similar to a power law because it shows no lines, and as we know well by now, we can use the redshift of spectral lines to determine the redshift of an AGN. But in this case, because of the blank appearance, it's not an easy task to accomplish. This, however, has been done by either finding a small number of very dim lines, or by making use of the high variability of the BL Lac, by doing observations at periods of very low activity of the nucleus. BL-Lac objects are low redshift objects in comparison to other AGNs, and measurements show redshifts including and under $z = 0.2$. They are also very scarse, and only a few hundred of them are found so far.[7, chapter 18.5]

OVV objects

Second class of similar objects are the optically, violently variable objects, or OVVs. Like BL Lacs, they also show strong variability in both radio and optical part of the spectrum, but with the important difference in that they also show strong and broad emission lines, exactly quasar-like. Difference is also seen in the redshifts of these objects, in comparison to the BL Lacs, as they are in the broader interval of $z = [0.1, 2]$.[7, chapter 18.5]

Blazars

Because of all the similarities, we can categorize the BL Lacs and the OVVs within one class of objects called blazars. This kind of categorization of objects under one general type is called unification, and more about it will be discussed in the incoming chapters. The characteristics Blazars show are high degrees of linear polarisation and something called superluminal motion, which we will explain in a bit. In the superluminal sources, the component of the radio source with small angular size is observed to separate at speeds greater than c. The reason for this relativistic motion is an angle of ejection being very close to the line of sight. We will go deeper in the problem in the next chapter. [7, chapter 18.5]

Superluminal motion and relativistic ballistic model

Relativistic balistic model is the simplest model for superluminal sources. The jet has multiple components that move along the same trajectory from the nucleus of AGN. Let's determine the kinematics of one observed relativistic component, and since all components look like radio beams, we shall call the observed one the beam.

- Initial coordinates:

    - D is distance from the observer to the source

    - θ is the angle between the beam and the observer

    - O is the origin from which the beam is ejected from

    - t_0 is time at which it has been ejected in the direction towards the observer

- Delay:

    - The signal from the beginning of the ejection arrives to observer's coordinates with delay $t_d = D/c$, because the light needs to travel the distance between the origin and the observer for the observer to observe it

- After certain time t_1:

    - Beam is at a distance vt_1 from O

    - Observer observes it at a projected distance $vt_1 sin\theta$ from his point of view

This means we can calculate the time when the light signal that carries this information arrives at the observer's coordinates

$$t_2 = t_1 + [(D - vt_1 \cos\theta)/c] \tag{5}$$

or to make it more obvious

$$t_2 - t_d = t_1 - \frac{vt_1 \cos\theta}{c} \tag{6}$$

We also need to calculate the new distance. The signal has to travel a shorter distance, $D - vt_1 cos\theta$, than the previous one D, that it needed for the initial signal at time t_o to reach the observer. From the time and the distance we get the speed. So, if we ask the observer, the $\perp$ component of the speed of the beam is:

$$v_\perp = \frac{vt_1 \sin\theta}{t_2 - t_d} = \frac{vt_1 \sin\theta}{t_1 - \frac{vt_1 \cos\theta}{c}} = \frac{v \sin\theta}{1 - \frac{v \cos\theta}{c}} \tag{7}$$

We get the maximum observed $\perp$ speed if we differentiate $v_\perp$ with respect to θ. With the value of an angle $\cos\theta = v/c$, the maximum speed is $v_{\perp,max} = \gamma v$, where $\gamma = (1 - \frac{v^2}{c^2})^{-\frac{1}{2}}$ is the Lorentz factor. The beam moves at a speed very close to the speed of light, and because of that, the apparent motions $v_\perp \gg c$ can be observed without violating causality and the postulates of special relativity. Superluminal motion is observed because the beam almost catches up with the radiation that it emits. To have superluminal motion, the line of sight between the observer and the beam needs to be very small, which is true for all blazars. [7, chapter 22.3]

2.2.5 LINERs and WLRGs

Fainter AGNs are known as Low Ionisation Nuclear Emission Regions or LINERs. In addition to spectra from H II region, most often they show narrow and faint emission lines from the central nuclear regions. Lower emission lines are sometimes strong, but lines of higher excitations are much fainter and not that broad. Galaxies classified as LINERS make up around 30% of all galaxies within the distances about 20–40 Mpc. It is still not clear if they should be a part of the AGN classification, but they look very similar to the objects classified as weak line radio galaxies (WLRG). In fact, the difference is that WLRGs show jet typical for RGs, but LINERs don't. This could potentially make them RQ version of WLRGs. [7, chapter 18.6] [18, page 4]

2.2.6 Ultra-Luminous Infrared Galaxies

Many galaxies with big star-forming regions are very strong sources of infrared (IR) emissions. The IR emission is coming from the dust, that is heated by the strong optical and UV rays. Some of these galaxies have very high IR luminosities, and are called Ultra-Luminous InfraRed Galaxies (ULIRGs). Around 1/2 of very luminous ULIGRs can be classified as a Seyferts, which are equally split in Seyferts of I and II type. The ones belonging in type I show BL emissions typical for such objects, but if we take redshift away, the lines look a lot like those of optically selected quasars of comparable non filtered luminosity, and hints at their nucleus being similar to such quasars. Most probable reason for strong IR emissions in ULIGRs is interactions of such galaxies with their neighbours. In the interacting regions, of such spiral galaxies, we can detect starbursts and the change in the interstellar gas. At times, the gas from this outer region is pushed into central nuclear region, containing the black hole, that feeds on the incoming gas, making such galaxy an active one.

2.3 Classification

2.3.1 AGNs by radio loudness

This first very basic classification of AGNs is by one of its properties called radio loudness, that we have seen in Seyfert and RGs, as well as in Quasars. This idea is to take the radio part of the EM spectrum, and divide AGNs in two groups, Radio Loud (RL) and Radio Quiet (RQ) AGNs. Depending on how visible and detectable they are in that part of the spectrum they almost all will fall into one of the two categories, regardless, there are some border cases. Looking at this type of classification, broad line radio galaxies (BLRG) are the radio-loud equivalent of Seyfert I galaxies, and narrow line radio galaxies (NLRG) are the radio-loud equivalent of Seyfert II galaxies. The RL nature of the RL sources is still not fully explained. The most probable reason for such asymmetry in the number of RL vs. RQ AGNs, where the number of RQ AGNs vastly supersides the number of RL ones (that make up not more than 15% of all AGNs) is the the one already mentioned while discussing RL and RQ quasars - the needed mass of the central black hole for each of the types. [18, pages 3, 4]

2.3.2 Fanaroff–Riley classification

Second important classification attempt was done by B. Fanaroff and J. Riley when they categorized certain selection of RL AGNs into two luminosity classes. AGNs with specific luminosity at 1.4 GHz of less than $10^{25}\mathrm{WHz}^{-1}$ are identified as FR I type, and those above the given threshold as FR II type. These limits between the types are also a morphological differences in the types. Let's for a moment ignore the fact that the nucleus is the brightest part of the AGN, and let's find the

second two radio brightest spots, each located on the one of the opposing sides of the objects. For the two AGNs that have the same full length L, we can have two totally different looking objects depending on the ratio of the distance D, between the emission's two second brightest spots, and the given L. FR I type objects have the ratio $\frac{D}{L}$ less than 0.5. At the same time, FR II objects have that same ratio greater than 0.5. That consequently makes any FR I more of a center bright type of radio object, and any FR II more of an edge bright radio object.
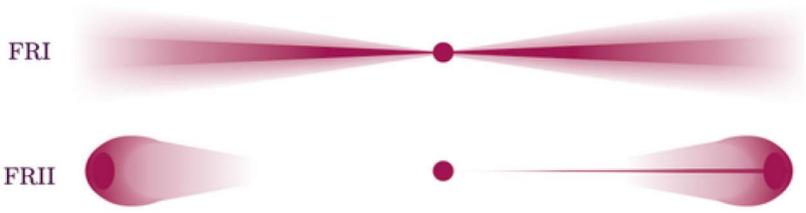

Figure 15: FR I and FR II morphology
[1, EmmaA]

Fanaroff–Riley Class 1 Morphology

FR I sources have the highest radio luminosity at the center of the jets, and it gets lower the more we move away from it. FR I galaxies mostly have two recognizable radio jets, that are sometimes curved. The BL-Lac objects can be classified as low-luminosity radio galaxies of FR I type.

Fanaroff–Riley Class 2 Morphology

FR IIs tend to have the highest radio luminosity at the ends of the lobes. FR II galaxies most often exhibit only one dominant jet, while the second jet is usually fainter, if not undetectable. The visible jet is almost always very straight in appearance. The OVV objects by type belong in the FR II category. [4, page 1207]
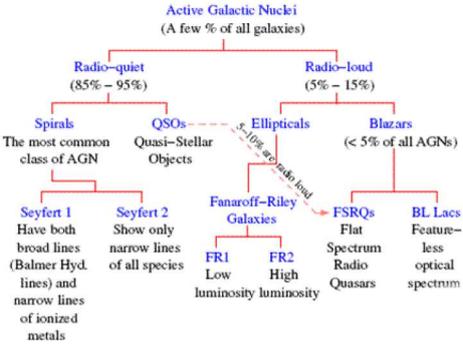

Figure 16: Classification Scheme of AGN
[7, online]

2.3.3   Unification Schemes

The concept of unification of AGNs under one type of object, resulted from the realisation that how the observer is oriented toward an AGN is important. If we could change our line of site, and consequently, the angle under which we observe the AGN, the observed properties would also change, because different features of AGN would become visible or obscured. There are multiple effects and physical barriers that cause the differences between the various classes of AGNs that we will discuss in an incoming chapters.
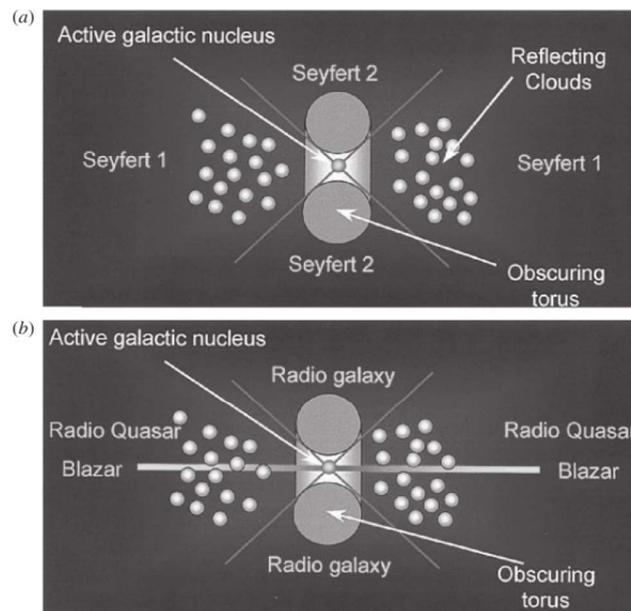
Seyfert Unification

Figure 17: a) Shows unification scheme of Seyfert I and II types determined by the angle between the observer and the galaxy b) Extends this unification to other types of AGNs
[7, page 604]

One such feature is the torus around the nucleus, which acts like a physical barrier, that bans clear view of the center of AGN, and makes direct observations of that region difficult. Such direct observation is only possible, if at the almost direct line of sight to the axis of the torus. The central region then becomes visible and we see AGN as Seyfert I type. The indirect observations of the same region are also possible, because on opposite sides of the torus (above and below the ring), is an area that contains reflective clouds made of dust and gas. This is the area of NL region, and it scatters radiation from the inner nuclear region. These waves that are reflected are being polarised by the scattering, but still show the same broad permitted spectral lines of type I that are broadened by high speed rotation of accretion disk of the black hole. What is also visible is the blue light and UV part of spectrum from the inner most region. In a case of a large angle to the line of sight, the nuclear regions are obscured, and so, only the narrow-line regions, which are on a bigger distance from the center, are observed directly. Since X-rays, especially higher energy ones, are not so easily absorbed by the torus, X-ray surveys were used to determine if this kind of unification makes sense. The surveys found no difference in the observed properties of Seyfert I and II type in this high energy part of the X-ray spectrum. At the same time, lower energy X-rays showed higher rate of absorption in Seyfert II type, making the obscuring torus highly plausible reason for differences observed in the two traditional Seyfert types. [7, p. 18.9.1]

Unification of Radio Galaxies and Radio Quasars

Another important type of unification of different types of AGNs is the one of radio galaxies and radio quasars. Both types often show extended radio features, unlike Seyfert galaxies, which makes attempt at unifying these objects the next logical step. Just like in Seyferts, where our line of sight was important for observing different properties, here we see the same pattern. But this time, the properties depend upon the angle at which the jet is observed. This type of unification could, if proved successful, also explain the existence of strong γ ray sources. Lets address some of the effects involved in this unification:

- Superluminal motions, that we described in the chapter regarding blazars, are found in lots of objects otherwise seen as compact RQuasars. For such motions to be observed, the relativistic jet needs to point almost directly toward the observer. This already gives hope of unifying blazars with RQuasars.

- Intensity of the dominant jet in radio quasars is observed as huge, because again, the jet points almost directly at the observer, blushifting the incoming waves towards higher frequencies. At the same time, the incoming waves from the faint jet on the opposite side, are being redshifted by pointing directly away from the observer. We already talked about such Doppler effect, but this further solidifies the arguments of relevance of the angle upon which the jet is observed.

- Next effect is the depolarisation asymmetry in the radio lobes. Depolarisation is the drop in the object's percentage of wave's polarisation that follows the drop in f of the observed wave. The drop is stronger on the faint jet side. That is because this side is pointing away from the observer, again, redshifting the waves to lower frequencies, that are more susceptible to this effect.

- The apparent sizes of the RQuasars are smaller than those of the radio RGs if both show similar z. This can be explained by the RGs being observed at a bigger angle to the line of sight than RQuasars. This again looks similar to the division of types between Seyferts resulting from different viewing angles.

- Lots of RGs' optical lines show linear polarisation from the scattering by the clouds in NL region. Again we see effects that can be explained in the same manner as in Seyfert galaxies.

Unification of most AGN classes

[7, p. 18.9.2] All these pieces of a puzzle show broader picture, if looked in a similar way as Seyfert galaxies, but now with the jet in sight. This time, the RQuasars are revealed when the central region is observed within the cone of around 90 degrees and the radio galaxies when the same regions are hidden by the obscuring torus. Radio jets are explained as collimated emissions by the nucleus. They are also probably powering the second radio extended feature - the radio lobes. In a meanwhile, the blazars are just AGNs where the jet is almost directly pointing at the observer, so emissions show relativistic effects, and the Doppler effect makes waves from these objects highly blueshifted. The SED of blazars show non-thermal emission and with two separate contributions present. The lower energy contribution from synchrotron emis- sion, and higher energy one from the inverse Compton (IC) emission. In the IC photons are upscattered to γ ray frequencies by the electrons within the jet.
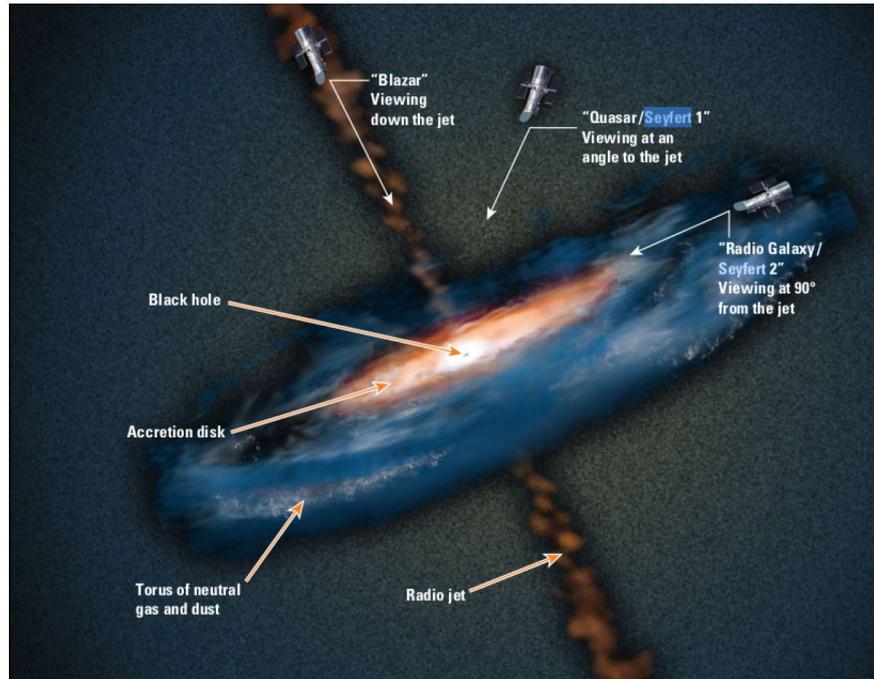
Figure 18: Unification scheme of AGN
[7, page 604]

3 Practical part

3.1 About this Blazar

Object S4 0954+65 is a blazar located at: R.A. (J2000): 09 58 47.00, Dec. (J2000): +65 33 55.00, that has been very hard to subclassify as FSRQ or BL Lac, and is still classified as a blazar of unknown type. At the same time, the redshift of a given blazar, $z = 0.3694$, had a measurement problem. This value has been used across different articles for years, but it wasn't reliable until recently, because of the long time inability to double measure it. The value of $z = 0.3694$ originates from the Fan and Cao 2004 article in which they got the value from the redshift of a detected H_α line, that was never again detected by other surveys. This ambiguity of redshift is very common for BL Lac objects, as they have very flat optical spectrum that shows almost no spectral lines. But as we said before, the measurement of width of the detected lines is needed to determine the redshift of AGN. And the detection of [MgII],[OIII], and [OII] spectral lines on 25th of May, 2015 was exactly what allowed to calculate similar redshift again in the article (Bracerra Gonzalez, 2020). The newly estimated redshift z = 0.3694 +/- 0.0011 is derived from the [Mg II] spectral line, along with two other values from the other lines: z = 0.3667 +/- 0.0003 derived from [OIII] line, and z = 0.3671 +/- 0.0003 from [OII] line.

Strong feature of this blazar is it's high variability in the visible part of the spectrum, that has been detected on multiple occasions, which is general characteristic of blazars.

Classification of this object was and still is very ambiguous. Mostly because the luminosity of BLR and torus, derived from one of the lines that was detected in optical part of the spectrum are strong enough to be consistent with the IR photon field which is needed to explain the IC process, and which would classify this object as more of the FSRQ rather than BL Lac. But, because certain observable quantities like apparent magnitude, point like images, spectrum without spectral lines that is very similar to power law, and gamma-ray emission characteristics, blazar S4 0954+ 65 was for years classified as BL Lac object.

The event of our interest is γ-ray burst that happened on 14/Feb/2015, as the highly increased gamma ray activity was detected, followed by increased flux of photons was in other parts of spectrum as well. I am here recreating light curves for different parts of spectrum, which we will explain in one of the later sections, as well as recreating SED plot. But for now, let's first take a look at the different instruments that collect data for the researchers.

3.2 Different Instruments That Cover Different Frequencies

3.2.1 MAGIC

Figure 19: The pair of telescopes on the right are the MAGIC telescopes

Major Atmospheric Gamma Imaging Cherenkov Telescopes (MAGIC) is a pair of Cherenkov telescopes placed on La Palma, in the Canary Islands, at 2200 m elevation. The pair makes a single measuring system called the MAGIC experiment. The experiment crew makes a huge international collaboration of around 160 scientists from 12 countries, one of which is also Croatia. The whole system with 2 mirrors reflects γ rays into very sensitive detector that it is mounted on an orientable frame. The radius of the mirror, of each telescope, is 8.5 m, which makes it the biggest reflector telescope of this kind. Because of a such large surface area of the mirror, it can detect γ rays in the range from 25 GeV to 30 TeV, despite it not being a space telescope. [16]

The light curve recreated from cited paper is for the day of the flare that is denoted with MJD 57067. The actual date is the night from 14/Feb/2015 to 15/Feb/2015, and it was very dark with no problematic light pollution. [8, page 13]

3.2.2 Fermi-LAT

Fermi is a γ-ray space telescope orbiting around Earth. It's primary detector is Large Area Telescope (LAT), detecting photons with energy from approximately 20 MeV to 300 GeV.
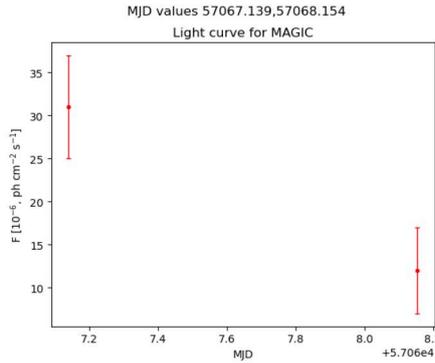
Figure 20: Recreated light curve for 2 data points collected by MAGIC

As we see MAGIC and Fermi-LAT have partial overlap in the energy they can detect, with Fermi-LAT generally being better at detecting lower, and therefore more likely to be absorbed by the Earth's atmosphere, frequencies, due to the fact that it's a space telescope.

The data points here taken by Fermi-LAT are part of the 3FGL catalogue, and were not taken specifically for the cited MAGIC paper. The cited MAGIC article uses the Fermi-LAT light curves for comparison to the MAGIC data, indicating elevated energies during certain dates. The data was not directly available in the cited MAGIC article, so the already made light curves are not recreated by me as well.

Value of best fit SED parametar called power-law spectral index is 1.87 ± 0.09 and was fixed in the model from the cited paper.[8, paragraph 4.2]

The source was detected, during (already observed by MAGIC) elevated energy state on 14/Feb/2015, by Fermi-LAT as well.

3.2.3   Neil Gehrels Swift Observatory

The table of measurements containing X-ray frequencies is gathered by the Swift's X-ray telescope. The whole observatory consists of 3 telescopes: Burst Alert Telescope detecting photons in range of 15 - 150 keV, X-ray Telescope with detection of 0.3 - 10 keV, and UV/optical Telescope with detection of 170 - 600 nm. It was sent to space by NASA in 2004 for the purpose of detecting and studying γ-ray bursts and it's afterglow that is in X, UV and optic range of wavelengths.

Swift mission, research, data storage and data analysis are executed by collaboration between United States that has Mission Operation Center, Italy with main ground station in Kenya that is being operated by Italian Space Agency, and United Kingdom that does data analysis in The Science Data Center and archive at the University of Leicester. [9]

The long term data collected by Swift is on the last page of the cited MAGIC article. It was used by me to reproduce light curves for long term Swift observation and for the dates when the flare was detected by different instruments, including MAGIC telescopes. For the range of MJD 56978.96395 or 17/Nov/2014 to 11/Mar/2015 March 11 or MJD 57092.26632 the avg.integral flux (that will be explained later in the section regarding light curves) for observed frequencies in this time period is double than the average flux outside of it. This means that the source had an increased X-ray activity, at the same time at which it had increased activity in high γ-ray frequencies. For the X-ray frequencies, spectral index was not constant and was in the range $1.15 \pm 0.06 \leq \gamma_X \leq 1.82 \pm 0.1$. The X-ray spectra on the night before and after the peak in observed γ-ray flare is presented as a power-law with spectral index of γ_X (Feb.13) = 1.82 ± 0.05 (χ^2/d.o.f. = 1.024/41) and γ_X (Feb.15) = 1.49 ± 0.07 (χ^2/d.o.f. = 1.025/24) respectively. The other instrument from Swift observatory, that is of our interest from Swift observatory, is the

Ultra-Violet and Optical Telescope (UVOT). The importance for us stands with the data collected by UVOT for 2016 article by Tanaka. The relevant data produces a light curve for already mentioned time period that is included in the light curve from the cited MAGIC article, but is not recreated by me. However, SED data points for this instrument I did include in my recreated SED.
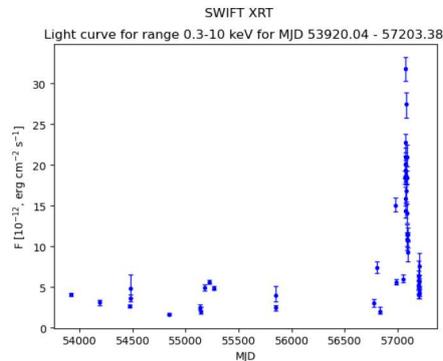

Figure 21: Recreated light curve for all available data points (0.3-10) keV collected by Swift XRT that shows the increase of the flux

3.2.4 Great Variety of Optical Instruments

Optical range of frequencies data was collected by lots of different instruments using different filters to filter certain frequencies, and some were used for polarimetric survey as well, which I will not recreate in this work. Instruments used are : 35 cm KVA telescope located on La Palma Island in Spain that collected data in the optical R band; [12] Perkins telescope of Lowell Observatory near the Arizona city of Flagstaff in the United States that is operated and owned by Boston University that uses it for its research. [11]; AZT-8 is Cassegrain type of telescope from 1964, at the Crimean Astrophysical Observatory in Nauchny. Telescope has a 70 cm parabolic primary mirror and 2 secondary mirrors that all together create Cassegrain system that puts focal point of telescope outside of the construction itself, and by doing so gives very long focal length despite relatively compact size of the telescope. [10]; 40 cm LX200 of St. Petersburg State University in Russia collected optical and part of the polarization data used in cited MAGIC article. [2],[8, page 6];
IAC80 is a telescope of 80 cm with CAMELOT (acronym in Spanish language for "Teide Observatory Light Improved Camera") direct CCD imager that collects optical data at the Teide Observatory at Tenerife. The same telescope was also used to collect part of the polarization data. [3]
The data analysis is coming from different papers, so the light curve will not be recreated by me for this part of the spectrum. But increase in flux was detected for the optical part of the spectrum at the same period as the February 2015 γ-ray flare. [8, page 6]

3.2.5 mm and Radio Surveys

POLAMI that stands for polarimetric monitoring of AGNs at millimetre wavelengths is focused on monitoring of the polarimetric properties of of 40 AGNs at 3.5 and 1.3 mm wavelengths. At the same time, the POLAMI database contains the data of over 200 AGNs, thanks to the different collaborations.
The instrument used is IRAM 30 m telescope that has 2 m secondary mirror and is located near Granada in Spain. The primary mirror is very large and telescope antenna weights 800 tons. [15]

24

Here we can clearly see how the size of the telescope has drastically increased when we moved away from the optical part of the spectrum towards radio part. The size was already great for high energy ray telescopes. But mostly either because they were actually in orbit around the Earth. Or, in case of the terrestrial gamma detector, the problem was that atmosphere was blocking lots of the rays, so the telescope needed large enough mirror to compensate for the loss. But in the case of the radio waves that are mostly not absorbed by our atmosphere, the problem becomes that observed wavelengths are huge, so we need large area to catch the radio waves.

Figure 22: IRAM 30m telescope

Even though the POLAMI data set in the article has a lot of data points, we will not be discussing this in a great detail, because our main focus is not the polarization, but building of light curves and SED of a given AGN. But still we need to mention that there is no great variability in this part of the spectrum that simultaneously corresponds to the MAGIC flare recorded on MJD 57067. [8, page 7]

Long term monitoring of this blazar is done by interferometry by Boston University using Very Long Baseline Array (VLBA). This long term monitoring at 43 GHz is used for studying the kinematics of the inner jet of the blazars where this one was also monitored few months after the γ-ray flare. [8, page]

The 3 new radio knots were found and the cited MAGIC article follows in detail the K15 knot, which is very compact in its size. Radio knot data is not part of the light curve creation so I will not go into the great details about this topic.

The 37 GHz (8 mm) data collection was made using telescope at Aalto University Metsähovi Radio Observatory and was part of the routine monitoring of the objects. This observatory specializes in long term monitoring of AGNs and these observations are done by researchers and students working at the observatory, while monitoring shifts are usually lasting one full week. During this period the personnel operates the radio telescope, and determines which sources should be observed based on priority events, weather conditions and other similar determining factors. Mostly observations are done remotely, and in periods of great weather conditions the telescope can be set to automatically do a short time observing survey. [17] Important fact is that while long term monitoring was done as much as the conditions were allowing, there is no simultaneous data available in the cited

MAGIC article set for this frequency, that is time corresponding to the gamma-ray flare detection. Still, a bigger flux was measured if making comparison of the data collected 1 day before and 1 day after the flare. [8, page 8]

Similar is true for the 40 m OVRO (Owens Valley Radio Observatory) that started monitoring program in 2008 but was sadly discontinued in 2020. While the program was still active, it was doing long term monitoring similar to Metsahovi Observatory, and it was capturing variability of this blazar at 15 GHz. Variability was detected for the time period of the flare, but nothing out of the ordinary if comparing these changes in flux to the ones outside of the dates of the flare. [14],[8, page 8]

3.3 Light Curves Explanation, Data and Code

Remember in section 2.1.5 when we were explaining SED of AGNs and needed to use a power law to calculate the energy flux? Well here, first we calculate the flux of incoming rays, but this time it is not something theoretically calculated, but is calculated from the data that was obtained through measurements. In general flux is calculated as:

$$\Phi = \frac{d^2 N}{dS dt} \tag{8}$$

which is basically a rate of the rays per unit area of a detector that are perpendicular to the area of detector itself. Differential energy spectrum is derivation of flux per energy:

$$\frac{d\Phi}{dE} = \frac{d^3 N}{dS dt dE} \tag{9}$$

So from differential energy flux by integration in the interval of the given energy band, we can calculate the Integral flux

$$\Phi_{100 to 200 GeV} = \int_{100 GeV}^{200 GeV} \frac{d\phi}{dE} dE \tag{10}$$

Light curve is just plot of evolution of integral flux over certain period of time, or simply, Φ vs. t plot. Light curves that I recreated show change over time, in the integral flux for Swift XRT and MAGIC data, caused by the flare detected in multiple wavelengths, that was detected by MAGIC telescopes on Feb 14th 2015. On the light curves stacked for MAGIC and Swift XRT, that share horizontal axis, we see a little delay in change of the flux for MAGIC data points. Similar delays were found by cited MAGIC article in most parts of the spectrum, while the original detection was in the optical part.

Explanation of the Python Code: SWIFT data table is an array that I created to be compatible with Python syntax using data available in the last page of the (MAGIC article). For each observation, identified by its date and Swift observation identifier, it is given next: the duration of the exposure, the integrated energy flux in 2 energy bands with error bars, spectral index of the best fit, the χ, and degrees of freedom of the fit. For recreating light curve I used integrated energy flux, it's error bars, and data about the time when the flux measurement was done in MJD format, for each observation. Using the table given in the article I created a python compatible array that I right after saved in a second, NumPy compatible array, which I also transposed for easier manipulation. From the big array, I saved the data I needed in the varables so it is easier for me to keep track of my own code. Since data was in character type I changed it back to float and using Matplotlib and NumPy libraries I created plots for lightcurves.

The code for all the light curves for SWIFT is similar, it just uses different data points to create plots. In a similar manner I recreated the code for 2 MAGIC data points available.
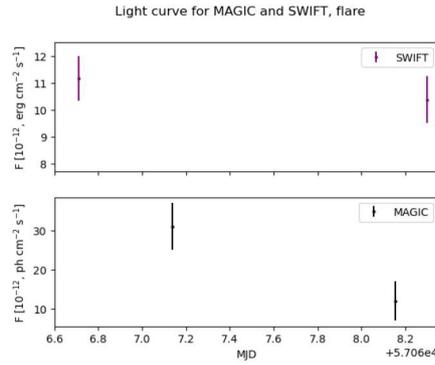
Figure 23: Light curves for MAGIC and Swift XRT for date of the flare and 2 surrounding dates
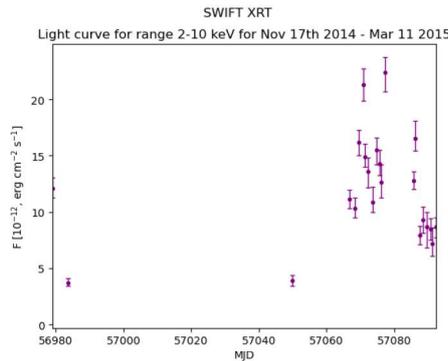

Figure 24: Light curve for Swift XRT from 17th Nov 2014 to 11th Mar 2015 date is showing flux changes over time, in months prior, at the time and for a month after the flame in the γ part of the spectrum.

3.4 SED of Blazar S4 0954+65

The SED of blazars is characterised by non-thermal emissions, and usually consists of two sections. The first of the components, the one lower in energy, represents synchrotron emission, and the high energy emission shows inverse Compton (IC) scattering. These terms were already explained in previous sections. In the IC, the photons are getting scattered to very high energies in γ part of the spectrum by electrons from the jet. The origin of the soft photon field is something we will not be getting into deeply, but important fact is that this origin varies depending on subclass of blazar in question. For majority of BL Lac blazars, the VHE emission can be nicely modeled through synchrotron IC emission. But, for the case of FSRQs, we also need external soft photon fields for the IC component. These photons are sometimes UV photons from BLR, and sometimes IR photons from the dusty torus. Since producing such complex models would be too complicated for this level of studies, I focused on creating reproduction of the SED plot using data table containing SED points for fig.7 from cited the MAGIC article. [8, pages 9, 10]

Recreated SED consists of multi-wavelength data collected by different instruments that were covered in section 3.2. This SED is created for the purpose of understanding first detected very high energy (VHE) flare of the blazar S4 0954+65 in February of 2015. Energy emission was first detected in the optical band, and was later picked up by other instruments in different parts of the spectrum. On the SED of given blazar we can clearly see some features that would be different if classification was different. Utter left part (Metsahovi, OVRO, POLAMI) is representative of how strongly present is syncrothron self absorption that makes difference between flat and steep
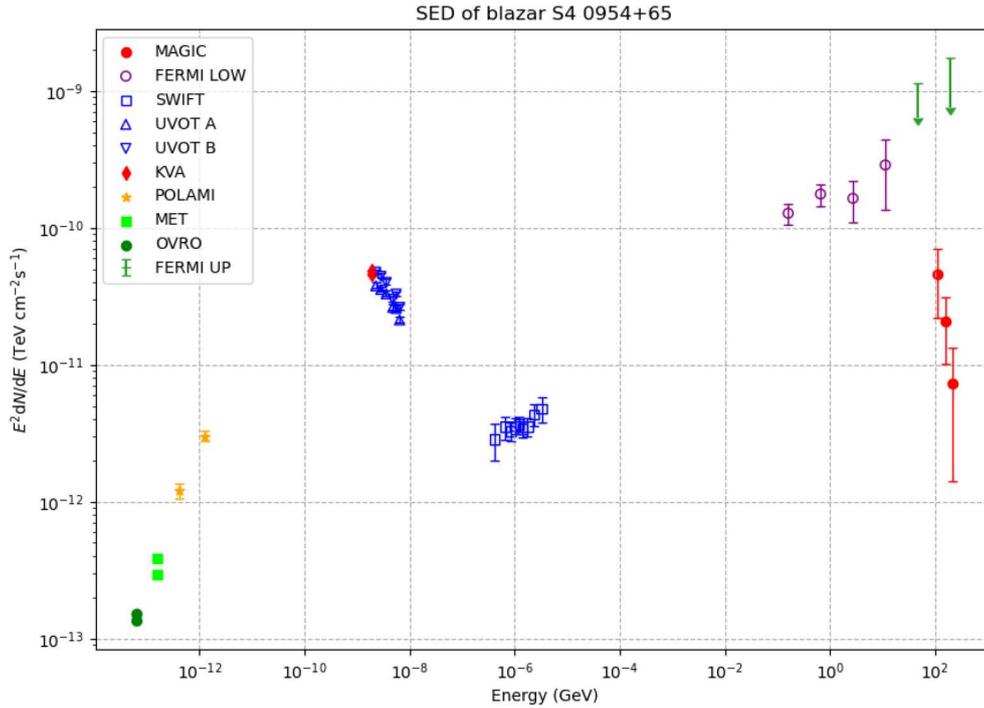
27

Figure 25: Recreated SED for blazar S4 0954+65

radio spectrum. The little more to the right side of this section is a simple powerlaw of Syncrotron radiation. VHE photons represent combination of IC emmision and Syncrotron radiation. SED also faintly shows presence of the of the BBB around the Swift data, feature that is mostly seen in FSRQs. Full Fit of SED can be seen on the original SED shown as figure 26 taken from the cited MAGIC article. [8, fig 7]
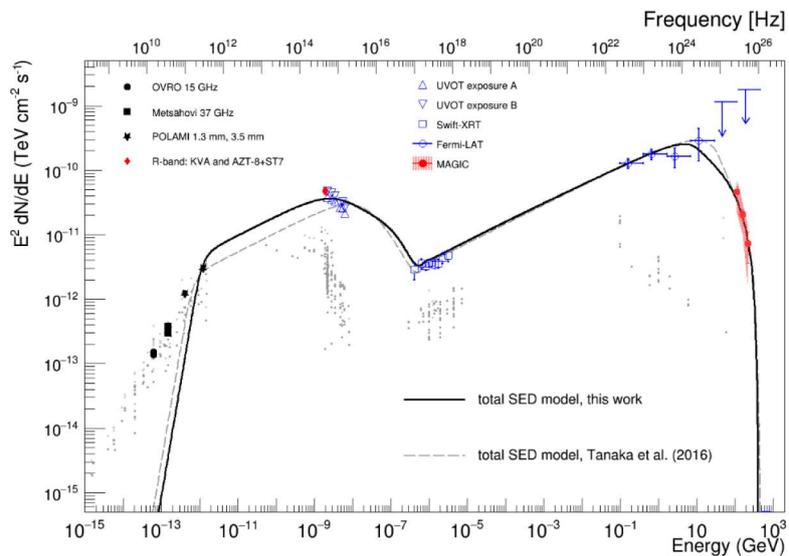

Figure 26: Original SED for blazar S4 0954+65 from the MAGIC article

Explanation of the Python Code The table of data for SED consists of 3 columns, 1st one being energy [GeV], second one SED [TeV cm$^{-2}s^{-1}$], and last one error bars for SED [TeV cm$^{-2}s^{-1}$].

I divided tables per instrument, and added needed syntax for tables to be in the format of a double list in python. I then created a function in python that makes transposed table with each of the previous columns being turned into rows for easier iteration. After that I added Matplotlib and NumPy libraries, and implemented syntax for the plot of SED. So we can see that, with data already provided, creating plots is a very straightforward task.

4 Conclusion

We can see that there isn't right or wrong way of classifying AGNs, but that in the end different classifications focus on different properties of objects. We have: broad-lines vs. narrow-lines, small angle vs. large angle, radio-loud vs. radio-quiet, extended features vs. no extended features, and so on. This makes a case for lots of divisions, but in making a classification one needs to, at the same time, search for the cause of these observed differences, and also stop to see what all AGNs have in common, like strong emissions across the spectrum, high compactness of the central region, and high "longevity". This way of thinking is more aligned with a goal of unifying AGNs. And even if the perfect unification is impossible for all objects, making this attempt helps further along. The reason being simply, that eliminating certain effects, caused by the point of view, makes room for exploring different reasons for the left over, not yet explained, differences. All AGNs, except LINERS, share similarities. But ambiguities in practical classification of AGNs show how much more there is to know about these objects. The same could be said for our given example of the Our blazar S4 0954+65 that shows how difficult, non straightforward and time dependent classification can be. Initially thought to be BL Lac it became clear in a few decades that is more of an transitional object with characteristics of FSRQ just as much as those of a BL Lac. [18, page 6] [8, paragraph 4.2] [19]

5 References

[1] Emma Alexander. *Resources*. URL: https://emmaalexander.github.io/resources.html. accessed: 12. 10. 2023.

[2] Boston University Institute for Astrophysical Research. *Resources*. URL: https://www.bu.edu/blazars/OPT.html. accessed: 10. 9. 2024.

[3] Boston University Institute for Astrophysical Research. *Resources*. URL: https://research.iac.es/OOCC/iac-managed-telescopes/iac80/camelot/. accessed: 10. 9. 2024.

[4] Dale A. Ostlie B.W. Carroll. *An Introduction to Modern Astrophysics*. Pearson Education Limited, 2014.

[5] M.R.S Hawkins. "Quasar variability: Correlations with amplitude". In: *Astronomy and Astrophysics Supplementary Series* 143.3 (2000), pp. 465–481. DOI: https://doi.org/10.1051/aas:2000190.

[6] S. Palen L. Kay and G. Blumenthal. *21st Century Astronomy*. Cambridge University Press, 2016.

[7] M. Longair. *High Energy Astrophysics*. Cambridge University Press, 2011.

[8] MAGIC Collaboration et al. "Detection of the blazar S4 0954+65 at very-high-energy with the MAGIC telescopes during an exceptionally high optical state". In: *Astronomy and Astrophysics Journal* 617 (2018), A30. DOI: 10.1051/0004-6361/201832624. URL: https://doi.org/10.1051/0004-6361/201832624. accessed: 12. 10. 2023.

[9] NASA. *Resources*. URL: https://swift.gsfc.nasa.gov/about_swift/. accessed: 08. 9. 2024.

[10] Crimean Astronomical Observatory. *Resources*. URL: https://crao.ru/en/telescopes-en/azt8-en. accessed: 10. 9. 2024.

[11] Perkins observatory. *Resources*. URL: https://www.bu.edu/pto/. accessed: 10. 9. 2024.

[12] Turola observatory. *Resources*. URL: https://users.utu.fi/kani/1m/. accessed: 08. 9. 2024.

[13] W.J. Kaufmann III R. Freedman. *Universe, 8th edition*. W. H. Freeman, 2008.

[14] Caltech education web site. *Resources*. URL: https://sites.astro.caltech.edu/ovroblazars/. accessed: 10. 9. 2024.

[15] IRAM official web site. *Resources*. URL: https://iram-institute.org/observatories/30-meter-telescope/. accessed: 10. 9. 2024.

[16] MAGIC official web site. *Resources*. URL: https://magic.mpp.mpg.de/. accessed: 8. 9. 2024.

[17] Metsahovi official web site. *Resources*. URL: https://www.aalto.fi/en/metsahovi-radio-observatory/active-galaxies. accessed: 10. 9. 2024.

[18] Clive Tadhunter. "An introduction to active galactic nuclei: classification and unification." In: *New Astronomy Reviews, by Elsevier* 52.6 (2008), pp. 227–239. DOI: https://doi.org/10.1016/j.newar.2008.06.004.

[19] TeVCat. *Resources*. URL: http://tevcat.uchicago.edu/?mode=1;id=258. accessed: 08. 9. 2024.

[20] H. Young and R. Freedman. *University Physics with Modern Physics*. Pearson Education, 2008.

6 Abbreviations

AGN = Active Galatic Nuclei

LINERS = Low-Ionisation Nuclear-Emmision Line Region

EM = Electromagnetic

SED = Spectral Energy Distribution

IR = Infrared

UV = Ultra Violet

FSRQ = Flat Spectrum Radio Quasar

FR = Fanaroff-Riley

RL = Radio Loud

RQ = Radio Quiet

RG = Radio Galaxy

RQuasar = Radio Quasar

WLRG = Weak Line Radio Galaxy

BLRG = Broad Line Radio Galaxy

NLRG = Narrow Line Radio Galaxy

BL = Broad Line

NL = Narrow Line

BBB = Big Blue Bump

IC = Inverse Compton

VLBA = Very Long Baseline Array

CAMELOT = Teide Observatory Light Improved Camera

OVRO = Owens Valley Radio Observatory

POLAMI = Polarimetric Monitoring of AGN at Millimeter Wavelengths

MET = Metsahovi

MAGIC = Major Atmospheric Gamma-Ray Imaging Cherenkov

IRAM = Institut de Radioastronomie Millimetrique

Fermi LAT = Fermi Large Area Telescope

LC = light curve

7 Biography

Tamara Radan was born on 8th of November od 1992. She graduated from the Secondary School of Science and Technology in Split, as part of a gymnasium class of 2011. Her hobbies include climbing and amateur telescope making.